Fluorescence Lifetime Imaging of Human Retinal Pigment Epithelium in Pentosan Polysulfate Toxicity Using Adaptive Optics Scanning Light Ophthalmoscopy

Kristen E. Bowles Johnson,[1–3] Janet A. H. Tang,[3,4] Karteek Kunala,[3] Khang T. Huynh,[3,5] Keith Parkins,[3] Qiang Yang,[3] and Jennifer J. Hunter[1,3,4,6]

[1]Flaum Eye Institute, University of Rochester, Rochester, New York, United States
[2]School of Optometry, Indiana University, Bloomington, Indiana, United States
[3]Center for Visual Science, University of Rochester, Rochester, New York, United States
[4]The Institute of Optics, University of Rochester, Rochester, New York, United States
[5]Department of Biomedical Engineering, University of Rochester, Rochester, New York, United States
[6]School of Optometry and Vision Science, University of Waterloo, Waterloo, Ontario, Canada

Correspondence: Kristen E. Bowles Johnson, Borish Center of Ophthalmic Research, 800 East Atwater Avenue, Bloomington, IN 47405, USA;
kbowlesj@iu.edu.

KK is now employed at Byers Eye Institute, Stanford University, Palo Alto, California, United States. KTH is now employed by the National Union of Healthcare Workers, California, United States. QY is now employed at the National Eye Institute, National Institutes of Health, Bethesda, Maryland, United States.

PURPOSE. Fluorescence lifetime ophthalmoscopy (FLIO) is an emerging clinical modality that could provide biomarkers of retinal health beyond fluorescence intensity. Adaptive optics (AO) ophthalmoscopy provides the confocality to measure fluorescence lifetime (FL) primarily from the retinal pigment epithelium (RPE) whereas clinical FLIO has greater influence from fluorophores in the inner retina and lens. Adaptive optics fluorescence lifetime ophthalmoscopy (AOFLIO) measures of FL in vivo could provide insight into RPE health at different stages of disease. In this study, we assess changes in pentosan polysulfate sodium (PPS) toxicity, a recently described toxicity that has clinical findings similar to advanced age-related macular degeneration.

METHODS. AOFLIO was performed on three subjects with PPS toxicity (57–67 years old) and six age-matched controls (50-64 years old). FL was analyzed with a double exponential decay curve fit and with phasor analysis. Regions of interest (ROIs) were subcategorized based on retinal features on optical coherence tomography (OCT) and compared to age-matched controls.

RESULTS. Twelve ROIs from PPS toxicity subjects met the threshold for analysis by curve fitting and 15 ROIs met the threshold for phasor analysis. Subjects with PPS toxicity had prolonged FL compared to age-matched controls. ROIs of RPE degeneration had the longest FLs, with individual pixels extending longer than 900 ps.

CONCLUSIONS. Our study shows evidence that AOFLIO can provide meaningful information in outer retinal disease beyond what is obtainable from fluorescence intensity alone. More studies are needed to determine the prognostic value of AOFLIO.

Keywords: pentosan polysulfate toxicity, fluorescence lifetime, adaptive optics (AO)

Measuring changes in fundus autofluorescence (FAF, i.e. fluorescence intensity) informs about retinal pigment epithelium (RPE) cellular health and is used to characterize, diagnose, and monitor outer retinal disease in the clinic. Fluorescence intensity provides insight into disease but lacks the ability to inform on bisretinoid composition. First formed in the photoreceptors, then accumulated in the RPE over a lifetime, bisretinoids are a collective byproduct of the visual cycle that includes N-retinylidene-N-retinylethanolamine (A2E), iso-A2E, and all-trans-retinal dimerphosophatidylethanolamine.[1,2] The bisretinoid composition, as many as 25 molecules identified,[2] and the molecular environment underlying FAF alterations can differ by genotype and disease.[3,4] For example, abnormal bisretinoid accumulation in photoreceptors and RPE cells, associated with loss of function mutations in the ABCA4 transporter gene, is hypothesized to be directly toxic to the neural retina and RPE.[5,6] In other conditions, such as retinitis pigmentosa, abnormal RPE lipofuscin accumulation is postulated to be secondary to increased photoreceptor cell death.[7] In age-related macular degeneration (AMD), quantitative fluorescence intensity decreases at an early stage of disease and remains reduced into late stage disease.[8–10]

Fluorescence lifetime (FL), a measure related to the time delay between fluorophore excitation and emission, is an imaging technique long used in microscopy that is now under investigation as a clinical tool. Clinical fluorescence lifetime ophthalmoscopy (FLIO; Heidelberg Spectralis, Heidelberg, Germany) measures FL simultaneously with FAF over the central 30 degrees of the retina. Clinical FLIO has shown changes in clinically normal retina[11] and many retinal diseases[12,13] including AMD.[11,14] Adaptive optics fluorescence lifetime ophthalmoscopy (AOFLIO) provides finer axial resolution (approximately 40 microns) than standard clinical FLIO techniques.[15,16]

In this study, we determine the ability of AOFLIO to identify a change in FL in disease and compare the FL from diseased retinas against the FL of exogenous forms of known retinal fluorophores in phasor space. Pentosan polysulfate sodium (PPS) toxicity, first described in 2018,[17] was chosen as the first cohort to determine utility of AOFLIO in RPE degeneration. PPS toxicity primarily involves the RPE and choriocapillaris[18] with hallmark retinal findings of parafoveal macular atrophy and a network of lattice-like RPE focal thickening corresponding to hyperfluorescent changes on FAF.[17] Although the bisretinoid composition underlying the fluorescence changes in PPS toxicity is not known, the retinal appearance is notably similar to AMD.[19,20] In this study, we sampled the FL of various retinal features in PPS toxicity that are typically associated with AMD.

METHODS

Subjects

This study was conducted according to the tenets of the Declaration of Helsinki and approved by the University of Rochester Research Subjects Review Board. In 2021 and 2022, three subjects (ages 57-67 years; Table 1) with a clinical diagnosis of PPS toxicity and a medical history of PPS use for 10 or more years were imaged with a high-resolution adaptive optics ophthalmoscope. High-resolution imaging was also performed on six age-matched normal controls (ages 50-64 years) for comparison. Age-matched controls underwent an initial screening in which no retinal pathology was found and did not have a medical history of systemic disease commonly associated with retinal disease. Age-matched controls were systematically imaged at 2, 8, and 12 degrees inferior and temporal to the fovea. Only extrafoveal locations were imaged in subjects with PPS toxicity ($n = 4$, 10, and 1 unique regions of interest for PPS 1-3, respectively). Foveal measures were not acquired in the subjects with PPS toxicity due to an inability to fixate simultaneously with the AOFLIO excitation beam on the fovea. Thus, foveal measurements in controls were excluded from analysis. All subjects had a refractive error less than ± 6 diopters (D) and cylinder less than 2 D.

Clinical Imaging

Prior to AOFLIO imaging, subjects PPS2 and PPS3 underwent clinical imaging including near-infrared (IR)

reflectance, FAF, and OCT on the Heidelberg Spectralis HRA (Heidelberg Engineering, Heidelberg, Germany) to determine regions of interest (ROIs). FAF imaging was obtained at least 24 hours before AOFLIO imaging to avoid overexposure of short-wavelength light. ROIs for PPS1 were predetermined based on prior clinical testing obtained at Flaum Eye Institute (Zeiss Cirrus, Dublin, CA, USA). Axial length was measured with the IOL Master (Zeiss, Dublin, CA, USA) and used for AOFLIO image scaling.

Adaptive Optics Scanning Light Ophthalmoscopy

Subjects underwent pupil dilation and cycloplegia with 2.5% phenylephrine and 1% tropicamide prior to imaging. An adaptive optics scanning light ophthalmoscope (AOSLO) designed for imaging human subjects was used, as previously described,[21,22] with modifications to obtain fluorescence lifetime.[23,24] After dilation, subjects sat with their head constrained by a chin and forehead rest and were asked to view a red fixation target that could be positioned within the viewing space to allow for imaging at predetermined ROIs across the central 28 degrees of the retina. Each location was imaged with a 1.4 degrees by 1.4 degrees field of view. Photoreceptor reflectance images (796 nm and <130 μW) were obtained simultaneously with fluorescence intensity and lifetime images of the RPE (excitation: 532Δ10 nm, <20 μW, $f_{laser} = 80$ MHz, 50 ps full-with half-max pulse; emission: 650Δ150 nm) in 30 second recordings. Compensation of longitudinal chromatic aberration between the 796 nm and 532 nm source was done by adding a 1D vergence difference at the eye.[25] This allowed simultaneous image collection of the photoreceptor mosaic (reflectance) and the RPE layer (fluorescence). Emitted photons were captured using a hybrid PMT (HPM-100-40; Becker & Hickl, Berlin, Germany) with a confocal pinhole of 2.3 Airy disk diameters that was automatically aligned for the greatest photon capture. For each photon, the time delay between the excitation pulse and captured emitted photon was measured in the temporal domain using commercial time-correlated single-photon counting (TCSPC) electronics and software (SPC-160 and SPCM; Becker & Hickl, Berlin, Germany).

Image Analysis

Data were desinusoided,[26] registered, and the forward and backward scans of each video were merged resulting in improved photon capture and accuracy at each pixel using custom software. The motion trace from the reflectance channel was used to register the corresponding fluorescence images. Transverse chromatic aberration between the reflectance and fluorescence images (796 nm vs. 532 nm light, respectively) was accounted for by segmenting each video into five or six sections and co-registering the fluorescence image to the reflectance image.[23] Video sections were registered individually before being combined at each pixel within the recording field of view (576 × 576 pixels). Lifetime data were exported as a TCSPC decay histogram of emitted photons within 256-time channels and analyzed in two ways; with a double exponential decay curve fit and with phasor analysis.[27,28] In this study, the double exponential decay curve fit was performed using a maximum likelihood estimation in SPCImage (version 8.1; Becker & Hickl). Curve fitting was performed with a kernel of 17 × 17 pixels and a threshold of 300 photons per TCSPC decay histogram. Thresholding was based on previously determined threshold limits.[29] A kernel size of 17 × 17 pixels is within the range

TABLE 1. PPS Toxicity Subject Demographics

Subject ID	Age, Y	Years on PPS
PPS1	57	15+
PPS2	67	10+
PPS3	62	20

of an RPE cell; 14 to 28 pixel diameters. Individual lifetime parameters were exported for additional analysis in MATLAB (Mathworks, Natick, MA, USA) and SigmaPlot (Systat version 14.5; Palo Alto, CA, USA). The weighted mean lifetime (τ_m) was calculated as previously described[24] using:

$$\tau_m = \frac{a_1\tau_1 + a_2\tau_2}{a_1 + a_2}$$

The Fourier transform of the TCSPC decay histogram at each pixel can also be evaluated in phasor space.[30] Phasor analysis was performed in MATLAB, as previously described.[31] In short, data were binned at a kernel size of 17 × 17 pixels and a threshold was set for 50 photons. Previous studies suggest that lower thresholds are acceptable for phasor analysis and have used a threshold as low as 37 photons.[27] An additional 3 ROIs met the criteria for analysis in phasor space that did not meet the criteria for exponential decay curve fitting resulting in a total of 15 ROIs analyzed by phasor analysis. A discrete Fourier transform was performed on binned data, evaluated at the repetition frequency of the laser, and plotted on a Cartesian scale (imaginary component versus real component, s versus g, respectively) along with the universal circle.[30] Short lifetimes lie on the right side of the phasor with g values close to one and prolonged lifetimes are toward the left with g values closer to zero. The phasor fingerprint, first termed the cell phasor,[32] is a set of phasor plots that can provide a comparison of underlying fluorescent molecules to a tissue sample. In this study, the FL of ROIs from PPS toxicity subjects and age-matched controls were compared to a previously described phasor fingerprint of well-known exogenous retinal fluorophores:[34] flavin adenine dinucleotide (FAD; Sigma; F6625), all-trans-retinal (at-ral, Sigma; R2500) synthesized exogenous A2E[33] and whole retinal extract of ABCA4 null pigmented mice (provided by Dr. Janet Sparrow).[3,34] In short, the exogenous fluorophores were dissolved in solution and imaged at the retinal plane of the AOFLIO system using UV-polymer cuvettes (Mfr. No. 759200; BrandTech Scientific, Inc., Essex, CT, USA).

Of note, the histograms of the double exponential decay curve fits of ROI pixels are notably different between Becker and Hickl software versions even when ensuring that curve fits are performed in the exact same manner with the same IRF curves. Previous publications[24] used Becker and Hickl SPCImage version 8.3 that resulted in a single peak distribution of τ_m for each ROI. In contrast, distributions of τ_m for each ROI from this study (analyzed with Becker and Hickl version 8.1), including normative data, were bimodal. Nonetheless, the observed differences between PPS toxicity and age-matched controls remained regardless of the software version used for analysis. However, these differences suggest that care should be taken to ensure that absolute comparisons are only made using a single version of SPCImage software. This difference did not affect phasor analysis, which was conducted using custom software.

RESULTS

PPS Clinical Characteristics

PPS toxicity subjects had a history of PPS use for more than 10 years (see Table 1) and had discontinued PPS at least 1 year prior to recruitment. For PPS1, clinical data from 2018 showed small areas of atrophy that progressed throughout follow-up examinations into 2022. PPS1 was the only subject to have previously undergone genetic screening for an inherited retinal degeneration. No causative mutations in genes associated with inherited retinal dystrophies were found. All subjects had changes on FAF and IR imaging extending greater than 10 degrees from the fovea. The phenotype of PPS1 and PPS2 was consistent with the disease spectrum first described and at least one area of complete retinal and RPE atrophy (cRORA).[17] The phenotype of PPS3 was more consistent with the recently described expanded phenotype characterization of PPS toxicity.[35] Fundus color photography, FAF, and IR imaging for each subject are shown in Figure 1.

### Multimodal AO Ophthalmoscopy in PPS Toxicity

A hallmark of PPS toxicity is parafoveal cRORA, similar to late-stage dry AMD. Example of OCT features typically associated with different stages of AMD within the ROIs imaged are shown in Figure 2A next to the corresponding photoreceptor mosaic (Fig. 2B), fluorescence intensity image (Fig. 2C), and fluorescence lifetime color map (Fig. 2D). FL of ROIs varied from slightly abnormal in areas without notable retinal alterations in the OCT B-scan (see Fig. 2, column D, row 2) to more pixels with prolonged FL in ROIs that contained focal RPE thickening/drusen (see Fig. 2, column D, row 3). ROIs with findings suggestive of greater RPE degeneration, such as hyper-reflective foci (HRF), incomplete outer retinal atrophy (iORA), or at the boarder of cRORA showed the longest lifetimes. Individual pixels in ROIs with RPE degeneration had Tau mean (τ_m) lifetimes close to 1000 ps. Although FL is independent of fluorescence intensity, hypofluorescent pixels can be more difficult to measure FL due to the low photon capture. Binned pixels with too few photons to fit a double exponential decay curve are seen as black within the FL image (see Fig. 2, column D, rows 2-6).

The phasor plot for the age-matched control's ROI is tightly compact suggesting a relatively homogeneous FL within the ROI (see Fig. 2, column E, row 1). In PPS toxicity ROIs without notable pathology on OCT B-scan, the phasor plot shows a slightly less homogenous FL by a less compact phasor in approximately the same location as the age-matched control ROI (see Fig. 2, column E, row 2). ROIs with pathology on OCT have greater variability of FL within the ROI and a trend toward lower g values showing a greater number of pixels with prolonged FL.

Double Exponential Decay Curve Fit Analysis

The double exponential decay curve fit parameters (τ_1, τ_2, and α_1) and mean lifetime (τ_m) of each pixel that met threshold within an ROI were represented by a histogram. Histograms from all imaged retinal locations were bimodal for τ_m, τ_1, and α_1. Peaks of the modes were termed short FL peak and long FL peak (see example in Fig. 3A). For all ROI histograms, τ_2 was unimodal. The lifetimes for the short and long FL peaks for τ_m and decay curve fit parameters were compared between the PPS toxicity ROIs and age-matched ROIs (see Fig. 2, Table 2.). The short FL peak and long FL peak of τ_m, τ_1, and the FL peak of τ_2 was prolonged in PPS subjects compared to age-matched controls (see Table 2). No
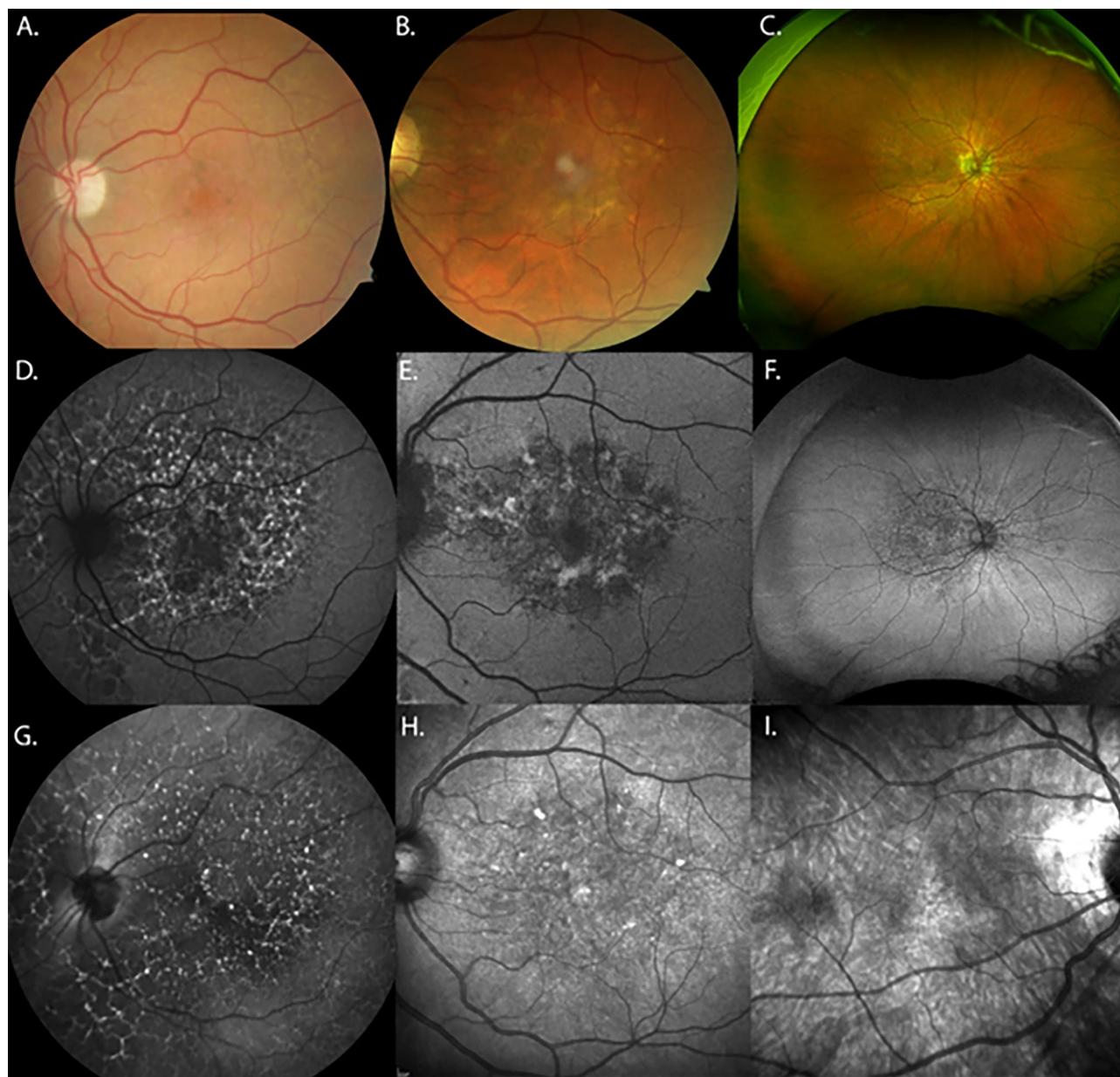
Figure 1. Clinical multimodal imaging of the PPS cohort. PPS1 (**A**, **D**, **G**) PPS2 (**B**, **E**, **H**) and PPS3 (**C**, **F**, **I**). Images include fundus color photography (**A–C**), FAF (**D–F**), and IR reflectance images (**G–I**).

difference was found between PPS toxicity and age-matched controls for $\alpha 1$ (see Table 2).

ROIs from PPS toxicity subjects were subcategorized into three groups: ROIs without disease features on OCT (see Fig. 3, green circles), ROIs with focal RPE thickening or drusen (see Fig. 3, yellow circles), and ROIs with RPE degeneration (HRF, iORA, and cRORA atrophic boarder; see Fig. 3, purple circles). ROIs containing HRF were grouped with ROIs containing retinal atrophy due to the high-risk association of HRF progression to cRORA.[36] The long FL peak of τ_m, τ_1, and τ_2 of PPS toxicity histograms showed a clear trend of greater FL prolongation with increasing ROI disease severity. For the long FL peak, ROIs with unremarkable OCT B-scans had lifetimes at the upper limit of the normal range to slightly outside the normal range. ROIs with focal RPE thick-

ening or drusen were outside the normal range with lifetimes slightly longer than ROIs without OCT findings. ROIs with RPE degeneration were prolonged compared to other PPS toxicity ROIs with the longest peak lifetimes reaching over 700 ps. The short lifetime peaks of τ_m and τ_1 were also prolonged compared to age-matched controls but appeared to have an "upper limit" at approximately the same timing as the lower limit of normal for the long FL peak (see Figs. 3B, 3C). In five ROIs with well demarcated RPE features (drusen, subretinal drusen deposits, and atrophy), the FL of surrounding pixels were compared to the pixels corresponding to the specific RPE feature. No trend between lifetimes of the surround and the RPE feature was seen. The percent difference in FL between the surround and RPE feature was minimal for all lifetime decay curve parameters.
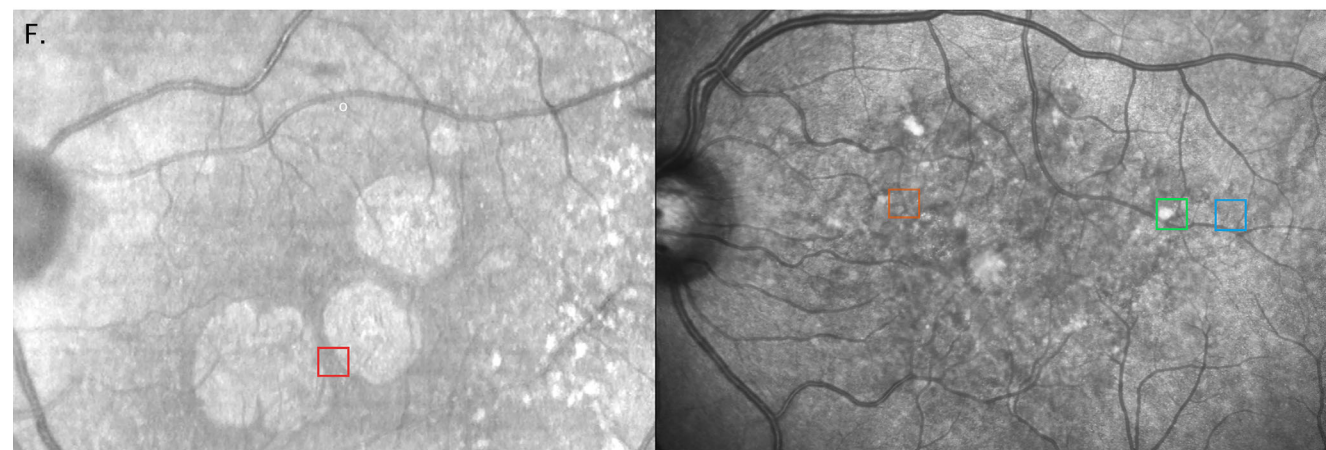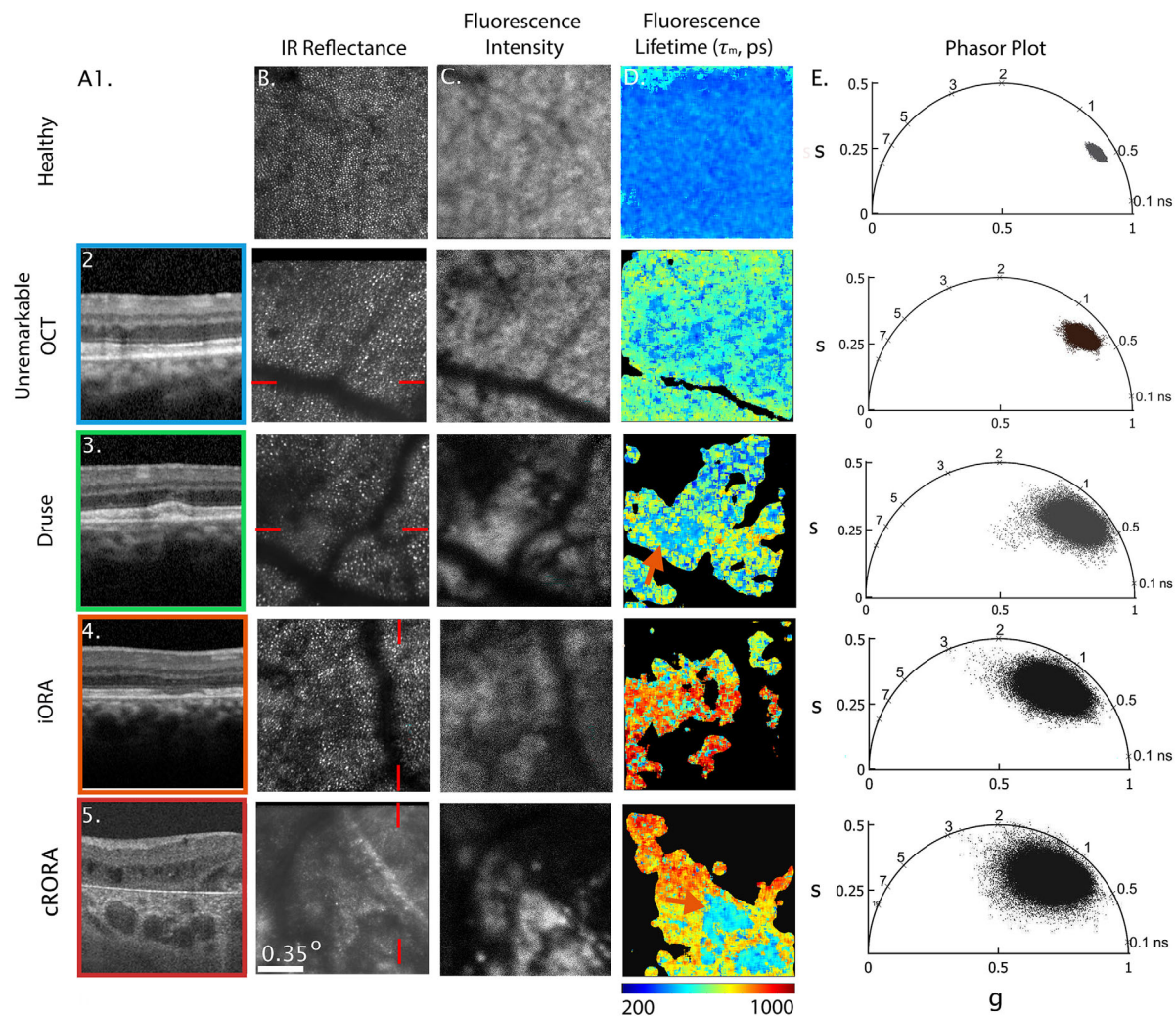
FIGURE 2. Representative lifetimes of various RPE pathologies visualized on OCT and AOSLO. OCT B-scans of the retinal feature are shown in *column A*. The B-scan image is surrounded by a color border that corresponds to colored boxes in the fundus images (F). The location of the B-scan within the ROI is indicated by the *vertical* or *horizontal red line* on the AOSLO photoreceptor mosaic (IR reflectance) image in *column B*. The photoreceptor mosaic, 532 nm fluorescence intensity of the RPE, and τ_m lifetimes are shown in *columns B to D*, respectively. The lifetime scalebar can be seen below *column D*. Black pixels in the lifetime images (*column D*) did not meet threshold for decay curve fitting. A phasor plot of each ROI is shown in *column E*. *Orange arrows* (column D, row 3, 5) mark areas of lifetimes with pronounced differences compared to the surrounding RPE.
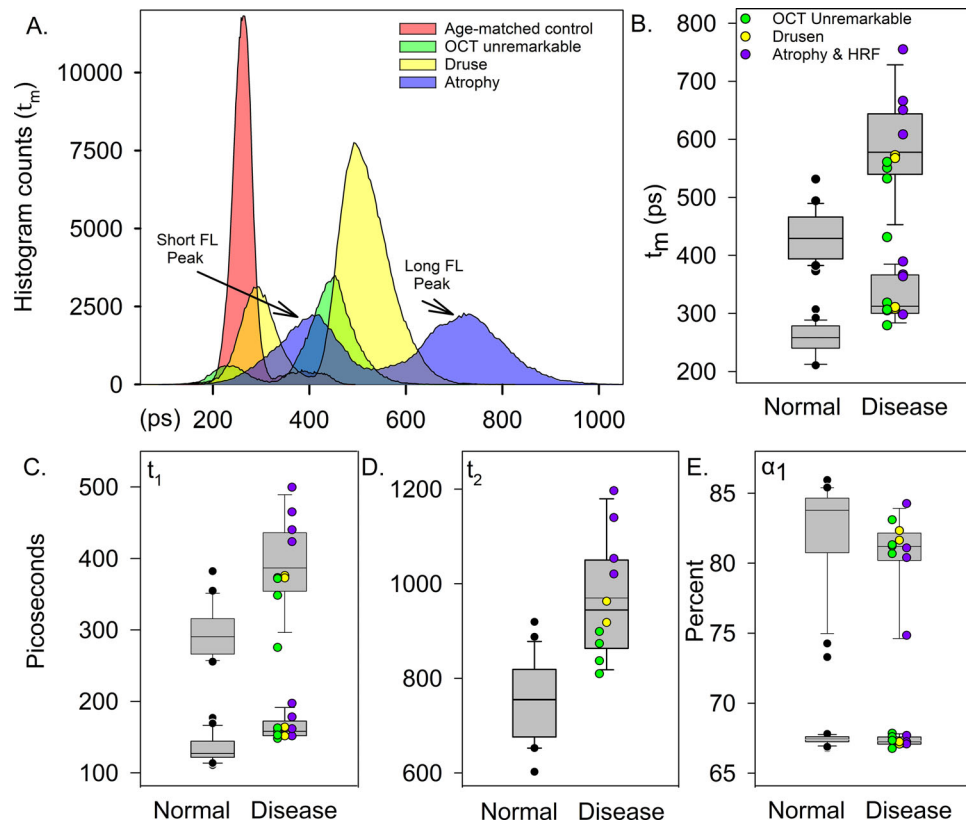
FIGURE 3. Example tau mean (τ_m) histograms and exponential decay curve fit parameter mode peak values of PPS toxicity ROIs compared to age-matched control ROIs. Histogram examples (**A**) show the range of tau mean (τ_m) values for all binned pixels from an ROI of an age-match control subject (*red*), from a normal appearing ROI on OCT B-scan in a PPS toxicity subject (*green*), PPS toxicity ROI with druse (*yellow*), and from an ROI at the border of retinal atrophy (*purple*). ROIs that contain retinal degeneration show larger shifts of τ_m values towards longer lifetimes. Histograms were bimodal for τ_m, τ_1, and α_1 of both normal and disease subjects. Lifetime mode peaks (i.e. short FL peak and long FL peak) of τ_m, τ_1, and α_1 are shown for each ROI (**B, C, E**, respectively) from age-matched controls (box and whisker plot, *left* with *black circles* marking peaks outside the interquartile range, short FL mode box and whisker plot inferior to long FL mode box and whisker plot) compared to subjects with toxicity (*right side*, short FL mode box and whisker plot inferior to long FL mode box and whisker plot). τ_2 was unimodal for all ROIs (**D**). Measures from PPS toxicity ROIs are subclassified into ROIs without disease on OCT (*green*), focal RPE thickening or drusen like deposits (*yellow*), and RPE degeneration (*purple*).

TABLE 2. Mean/Median and Standard Deviation/Quartiles for Double Exponential Decay Curve Fit Parameters for Each Cohort and Subgroup

Group	Short Lifetime Peak			Long Lifetime Peak		
	Mean Median	(SD) 25%/75%	Difference	Mean Median	(SD) 25%/75%	Difference
Tau mean						
Age matched controls ($n = 22$)	255.3	(22.0)	65.1	434.1	(42.2)	151.1
PPS toxicity ($n = 12$)	320.4	(33.1)		585.2	(83.7)	
Unremarkable OCT and Drusen ($n = 6$)	302.4	292.2/309.2	44.1	500.9	512/571	143.1
Atrophy and hyper-reflective foci ($n = 6$)	346.5	301.2/370.1		644	599.5/704.1	
Tau 1						
Age matched controls	127.1	121.7/144.2	32	300.0	(30.0)	106.5
PPS toxicity	160	152.0/172.4		406.5	(54.2)	
Unremarkable OCT and Drusen	156.7	150.8/157.8	15.1	376.9	348.8/391	67.2
Atrophy and hyper-reflective foci	171.8	153.3/181.1		444.1	412.0/473.7	
Tau 2						
Age matched controls				755.8	(84.0)	211.7
PPS toxicity				967.5	(123.3)	
Unremarkable OCT and Drusen				912.3	873.6/931.8	145.8
Atrophy and hyper-reflective foci				1058.1	990.3/1179.1	
Alpha 1						
Age matched controls	67.4	(0.27)	0.124	83.0	(1.0)	0.5
PPS toxicity	67.3	(0.31)		82.4	(1.6)	

The median with 25% and 75% quartiles for decay curve fitted values are reported for groups with non-normal distribution.
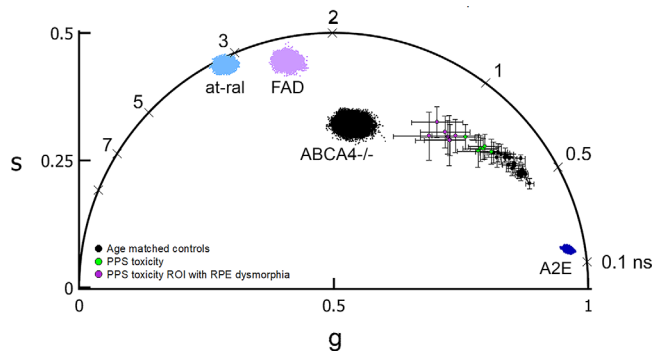
FIGURE 4. Phasor plot with lifetime center of mass ±SD of age-matched control ROIs (*black*) compared to ROIs of PPS toxicity subjects without OCT retinal features and focal RPE thickening or drusen (*green*) and ROIs with RPE degeneration/dysmorphia(*magenta*). Human AOFLIO data is compared against the FL of extracts[34] as labeled and whole retinal extract from an ABCA4 null pigmented mouse.

Phasor Analysis Center of Mass Compared to Exogenous Fluorophores

Assessment of FL in phasor space has the potential to determine the relative distribution of the underlying fluorophore composition that influences the FL measured from a living tissue.[32] Figure 4 shows the center of mass of all ROIs from PPS toxicity and age-matched control subjects compared to previously described exogenous fluorophores: A2E, all-trans-retinal, and FAD.[34] The FL of ABCA4 null mouse whole retinal extract[34] is also plotted as an example of the FL position of a well-characterized outer retinal disease. PPS toxicity subjects had prolonged lifetimes in phasor space compared to age-matched controls (g median = 0.73, interquartile range [IQR] = 0.71–0.80 vs. 0.86, IQR = 0.84–0.87, s median = 0.28, IQR = 0.27–0.30 vs. 0.24, IQR = 0.23–0.26, PPS versus controls). The FL of age-matched controls was closer to the exogenous fluorophore A2E. This suggests that RPE changes in PPS toxicity may have a larger relative contribution of fluorophores other than A2E compared to age-matched controls, and more similar to the FL of ABCA4 null mice whole retinal extracts. ROIs of PPS toxicity were grouped as ROIs with clinical evidence of RPE degeneration/dysmorphia (magenta) and other ROIs (green). The altered ratio of A2E to other contributing fluorophores was exaggerated in ROIs with RPE degeneration/dysmorphia.

Discussion

PPS is the only oral treatment for interstitial cystitis approved by the US Food and Drug Administration. It's mechanism of action is hypothesized to reduce bladder pain by increasing the glycosaminoglycan/mucin barrier covering the bladder epithelium.[37] PPS shares many properties with heparin sulfate.[38] PPS associated retinal toxicity could be due to an alteration of glycosaminoglycan concentration or activity within the photoreceptor extracellular matrix (ECM) and other ocular tissues with a rich presence of heparin sulfate, such as Bruch's membrane and choroidal blood vessels.[39] Alterations in the photoreceptor ECM have also been implicated in AMD.[40–42]

In this study, we found that in vivo measures of FL of the RPE of PPS toxicity subjects had prolonged FL compared to age-matched controls. The exact changes in lipofuscin composition or environment that contribute to prolonged FL in retinal disease remains elusive. Analysis of fluorophores in phasor space could provide some context for underlying fluorophores. Toward this goal, this study compared the FL of disease and older normal subjects to a limited number of exogenous fluorophores in phasor space. FL in subjects with PPS toxicity showed a center of mass closer to the FL from *ABCA4* null mice whole retinal extracts, suggesting a smaller contribution from A2E compared to age-matched control subjects. The altered ratio of A2E to other contributing fluorophores was exaggerated in ROIs with RPE degeneration. These findings suggest that a greater proportion of fluorophores, such as all-trans-retinal and FAD, could be influencing the FL from PPS toxicity ROIs. A drawback of this analysis is that the exogenous molecules measured in phasor space are inherently different than the environment and compositional makeup of the molecules within the RPE and neural retina in vivo. In addition, the inclusion of whole neural retina in the sample from ABCA4 null mouse could lead to a greater contribution of FL from FAD than would be expected in FL with AOFLIO. However, this study provides a rudimentary understanding of the origins of FL signatures in PPS toxicity. The work by Ami et al in hyperspectral autofluorescence imaging suggest at least 3 independent fluorophores in the RPE.[43] It is possible that prolonged lifetimes in PPS toxicity is attributable to increased melanolipofuscin, which is known to increase with age and in AMD[44] but is not obtainable in an exogenous form. Prolonged lifetimes in AMD RPE cells have also been hypothesized to be associated with increased oxidative stress.[45,46]

PPS toxicity has not been characterized with clinical FLIO, but different stages of AMD[11,46] and retinal features in AMD eyes have been characterized with clinical FLIO.[14,47] Clinical FLIO has a shorter excitation wavelength than AOFLIO (473 nm vs. 532 nm) with an emission collection bandwidth in the long spectral channel comparable to AOFLIO. Similar to ROIs of PPS retina without features of disease on OCT, clinical FLIO has shown alterations in FL in clinically normal retinal locations of subjects with age-related changes, such as drusen.[11] Our finding that retinal locations with HRF was associated with prolonged FL is consistent with clinical FLIO findings.[47] Clinical FLIO studies typically report lifetimes for RPE atrophy.[48] However, pixels corresponding to RPE atrophy did not contain sufficient photons for analysis in AOFLIO. This inconsistency could be due to increased confocality in AOFLIO compared to clinical FLIO, which assesses FLIO of the retina in it's entirety and is influenced by fluorophores of the ocular lens.

A short coming of our study is the small cohort (*n* = 3). However, even with a small cohort, an obvious trend of prolonged lifetimes in ROIs with greater RPE degeneration is seen.

AO ophthalmoscopy has revolutionized human subject research in part due to the ability to measure changes in individual cells in the retina. However, resolving RPE cells with fluorescence intensity is not always possible even in normal individuals, especially in the parafovea.[23] Another reason why RPE cells were rarely resolved in this study could be that PPS toxicity typically affects the parafoveal region in early toxicity. Likewise, loss of RPE structural integrity resulting in a loss of RPE cell visibility with fluorescence intensity has also been reported in AMD.[25]

Recently, Weber et al. showed that subretinal drusen deposits had increased FL compared to the surrounding RPE with clinical FLIO.[48] The lack of differences between lifetimes in RPE surround versus well demarcated RPE features in AOFLIO could be due to the limited data set and requires investigation of specific RPE pathologies. Our study did not have enough data to determine AOFLIO signatures of a specific retinal feature. However, some ROIs showed dramatic and somewhat surprising changes in AOFLIO. For example, Figure 2, column D, row 3 (arrow) shows a hyperfluorescent drusen-like deposit with qualitatively shorter FL compared to the surround. This finding is consistent with drusen without hyperpigmentation in intermediate AMD seen with clinical FLIO.[49] A significant shortening of FL was also associated with hyperfluorescence material at the RPE atrophic border compared to the prolonged lifetimes of the surrounding RPE (see Fig. 2, column D, row 7, arrow).

We found that imaged RPE in PPS toxicity subjects had prolonged FL compared to age-matched controls. ROIs with RPE degeneration showed longer FLs than ROIs with RPE focal thickening or no pathology. Our study shows that AOFLIO can provide additional information about RPE beyond fluorescence intensity alone and sets a basis to study FL in larger cohorts to determine it's full prognostic value.

Disclosure: **K.E. Bowles Johnson**, None; **J.A.H. Tang**, None; **K. Kunala**, None; **K.T. Huynh**, None; **K. Parkins**, University of Rochester (P); **Q. Yang**, University of Rochester (P), Canon Inc. (P), Montana State University (P); **J.J. Hunter**, University of Rochester (P)

References

1. Ng KP, Gugiu B, Renganathan K, et al. Retinal pigment epithelium lipofuscin proteomics. *Mol Cell Proteomics*. 2008;7:1397–1405.
2. Sparrow JR, Gregory-Roberts E, Yamamoto K, et al. The bisretinoids of retinal pigment epithelium. *Prog Retin Eye Res*. 2012;31:121–135.
3. Kim SR, Fishkin N, Kong J, Nakanishi K, Allikmets R, Sparrow JR. Rpe65 Leu450Met variant is associated with reduced levels of the retinal pigment epithelium lipofuscin fluorophores A2E and iso-A2E. *Proc Natl Acad Sci USA*. 2004;101:11668–11672.
4. Ablonczy Z, Smith N, Anderson DM, et al. The utilization of fluorescence to identify the components of lipofuscin by imaging mass spectrometry. *Proteomics*. 2014;14:936–944.
5. Sparrow JR, Marsiglia M, Allikmets R, et al. Flecks in recessive Stargardt disease: short-wavelength autofluorescence, near-infrared autofluorescence, and optical coherence tomography. *Invest Ophthalmol Vis Sci*. 2015;56:5029–5039.
6. Song H, Rossi EA, Latchney L, et al. Cone and rod loss in Stargardt disease revealed by adaptive optics scanning light ophthalmoscopy. *JAMA Ophthalmol*. 2015;133:1198–1203.
7. Schuerch K, Woods RL, Lee W, et al. Quantifying fundus autofluorescence in patients with retinitis pigmentosa. *Invest Ophthalmol Vis Sci*. 2017;58:1843–1855.
8. Chandra S, Grewal MK, Gurudas S, et al. Quantitative autofluorescence in non-neovascular age related macular degeneration. *Biomedicines*. 2023;11:560.
9. Gliem M, Müller PL, Finger RP, McGuinness MB, Holz FG, Charbel Issa P. Quantitative fundus autofluorescence in early and intermediate age-related macular degeneration. *JAMA Ophthalmol*. 2016;134:817–824.
10. Bindewald A, Bird AC, Dandekar SS, et al. Classification of fundus autofluorescence patterns in early age-related macular disease. *Invest Ophthalmol Vis Sci*. 2005;46:3309–3314.
11. Sauer L, Gensure RH, Andersen KM, et al. Patterns of fundus autofluorescence lifetimes in eyes of individuals with nonexudative age-related macular degeneration. *Invest Ophthalmol Vis Sci*. 2018;59:Amd65–Amd77.
12. Dysli C, Wolf S, Hatz K, Zinkernagel MS. Fluorescence lifetime imaging in Stargardt disease: potential marker for disease progression. *Invest Ophthalmol Vis Sci*. 2016;57:832–841.
13. Jaggi D, Solberg Y, Dysli C, et al. Fluorescence lifetime imaging ophthalmoscopy as predictor of long-term functional outcome in macula-off rhegmatogenous retinal detachment. *Retina (Philadelphia, Pa)*. 2022;42:2388–2394.
14. Dysli C, Fink R, Wolf S, Zinkernagel MS. Fluorescence lifetimes of drusen in age-related macular degeneration. *Invest Ophthalmol Vis Sci*. 2017;58:4856–4862.
15. Mainster MA, Desmettre T, Querques G, Turner PL, Ledesma-Gil G. Scanning laser ophthalmoscopy retroillumination: applications and illusions. *Int J Retina Vitreous*. 2022;8:71.
16. Lu R, Aguilera N, Liu T, et al. In-vivo sub-diffraction adaptive optics imaging of photoreceptors in the human eye with annular pupil illumination and sub-Airy detection. *Optica*. 2021;8:333–343.
17. Pearce WA, Chen R, Jain N. Pigmentary maculopathy associated with chronic exposure to pentosan polysulfate sodium. *Ophthalmology*. 2018;125:1793–1802.
18. Abou-Jaoude MM, Davis AM, Fraser CE, et al. New insights into pentosan polysulfate maculopathy. *Ophthalmic Surg Lasers Imaging Retina*. 2021;52:13–22.
19. Mukhopadhyay C, Boyce TM, Gehrs KM, et al. Age-related macular degeneration masquerade: a review of pentosan polysulfate maculopathy and implications for clinical practice. *Asia Pac J Ophthalmol (Philadelphia, Pa)*. 2022;11:100–110.
20. Lyons RJ, Brower J, Jain N. Visual function in pentosan polysulfate sodium maculopathy. *Invest Ophthalmol Vis Sci*. 2020;61:33.
21. Dubra A, Sulai Y. Reflective afocal broadband adaptive optics scanning ophthalmoscope. *Biomed Opt Express*. 2011;2:1757–1768.
22. Zhang J, Yang Q, Saito K, Nozato K, Williams DR, Rossi EA. An adaptive optics imaging system designed for clinical use. *Biomed Opt Express*. 2015;6:2120–2137.
23. Granger CE, Yang Q, Song H, et al. Human retinal pigment epithelium: in vivo cell morphometry, multispectral autofluorescence, and relationship to cone mosaic. *Invest Ophthalmol Vis Sci*. 2018;59:5705–5716.
24. Tang JAH, Granger CE, Kunala K, et al. Adaptive optics fluorescence lifetime imaging ophthalmoscopy of in vivo human retinal pigment epithelium. *Biomed Opt Express*. 2022;13:1737–1754.

25. Rossi EA, Rangel-Fonseca P, Parkins K, et al. In vivo imaging of retinal pigment epithelium cells in age related macular degeneration. *Biomed Opt Express*. 2013;4:2527–2539.

26. Yang Q, Yin L, Nozato K, et al. Calibration-free sinusoidal rectification and uniform retinal irradiance in scanning light ophthalmoscopy. *Opt Lett*. 2015;40:85–88.

27. Digman MA, Caiolfa VR, Zamai M, Gratton E. *The phasor approach to florescence lifetime imaging: Exploiting phasor linear properties*. Irvine, CA: UC Irvine; 2012. Issue 2, L14–L16.

28. Digman MA, Caiolfa VR, Zamai M, Gratton E. The phasor approach to fluorescence lifetime imaging analysis. *Biophys J*. 2008;94:L14–L16.

29. Nasser M, Meller A. Lifetime-based analysis of binary fluorophores mixtures in the low photon count limit. *iScience*. 2022;25:103554.

30. Malacrida L, Ranjit S, Jameson DM, Gratton E. The phasor plot: a universal circle to advance fluorescence lifetime analysis and interpretation. *Annu Rev Biophys*. 2021;50:575–593.

31. Huynh KT, Walters S, Foley EK, Hunter JJ. Separate lifetime signatures of macaque S cones, M/L cones, and rods observed with adaptive optics fluorescence lifetime ophthalmoscopy. *Sci Rep*. 2023;13:2456.

32. Stringari C, Cinquin A, Cinquin O, Digman MA, Donovan PJ, Gratton E. Phasor approach to fluorescence lifetime microscopy distinguishes different metabolic states of germ cells in a live tissue. *Proc Natl Acad Sci USA*. 2011;108:13582–13587.

33. Parish CA, Hashimoto M, Nakanishi K, Dillon J, Sparrow J. Isolation and one-step preparation of A2E and iso-A2E, fluorophores from human retinal pigment epithelium. *Proc Natl Acad Sci USA*. 1998;95:14609–14613.

34. Tang JAH. Characterizing and identifying the fluorescence lifetime of the in vivo human RPE cellular mosaic. *The Institute of Optics*. University of Rochester ProQuest Dissertations Publishing: University of Rochester; 2023.

35. Jain N, Liao A, Garg SJ, et al. Expanded clinical spectrum of pentosan polysulfate maculopathy: a macula society collaborative study. *Ophthalmol Retina*. 2022;6:219–227.

36. Duic C, Pfau K, Keenan TDL, et al. Hyperreflective foci in age-related macular degeneration are associated with disease severity and functional impairment. *Ophthalmol Retina*. 2023;7:307–317.

37. Pantazopoulos D, Karagiannakos P, Sofras F, Kostakopoulos A, Deliveliotis C, Dimopoulos C. Effect of drugs on crystal adhesion to injured urothelium. *Urology*. 1990;36:255–259.

38. Smith MM, Melrose J. Pentosan polysulfate affords pleotropic protection to multiple cells and tissues. *Pharmaceuticals (Basel)*. 2023;16:437.

39. Clark SJ, Keenan TD, Fielder HL, et al. Mapping the differential distribution of glycosaminoglycans in the adult human retina, choroid, and sclera. *Invest Ophthalmol Vis Sci*. 2011;52:6511–6521.

40. Cao L, Wang H, Wang F, Xu D, Liu F, Liu C. Aβ-induced senescent retinal pigment epithelial cells create a proinflammatory microenvironment in AMD. *Invest Ophthalmol Vis Sci*. 2013;54:3738–3750.

41. Piskova T, Kozyrina AN, Di Russo J. Mechanobiological implications of age-related remodelling in the outer retina. *Biomater Adv*. 2023;147:213343.

42. Zhou J, Ueda K, Zhao J, Sparrow JR. Correlations between photodegradation of bisretinoid constituents of retina and dicarbonyl adduct deposition. *J Biol Chem*. 2015;290:27215–27227.

43. Ben Ami T, Tong Y, Bhuiyan A, et al. Spatial and spectral characterization of human retinal pigment epithelium fluorophore families by ex vivo hyperspectral autofluorescence imaging. *Transl Vis Sci Technol*. 2016;5:5.

44. Kotnala A, Senthilkumari S, Wu G, et al. Retinal pigment epithelium in human donor eyes contains higher levels of bisretinoids including A2E in periphery than macula. *Invest Ophthalmol Vis Sci*. 2022;63:6.

45. Brown EE, DeWeerd AJ, Ildefonso CJ, Lewin AS, Ash JD. Mitochondrial oxidative stress in the retinal pigment epithelium (RPE) led to metabolic dysfunction in both the RPE and retinal photoreceptors. *Redox Biol*. 2019;24:101201.

46. Feldman TB, Yakovleva MA, Larichev AV, et al. Spectral analysis of fundus autofluorescence pattern as a tool to detect early stages of degeneration in the retina and retinal pigment epithelium. *Eye (London, England)*. 2018;32:1440–1448.

47. Hammer M, Jakob-Girbig J, Schwanengel L, et al. Progressive dysmorphia of retinal pigment epithelium in age-related macular degeneration investigated by fluorescence lifetime imaging. *Invest Ophthalmol Vis Sci*. 2021;62:2.

48. Weber S, Simon R, Schwanengel LS, et al. Fluorescence lifetime and spectral characteristics of subretinal drusenoid deposits and their predictive value for progression of age-related macular degeneration. *Invest Ophthalmol Vis Sci*. 2022;63:23.

49. Schwanengel LS, Weber S, Simon R, et al. Changes in drusen-associated autofluorescence over time observed by fluorescence lifetime imaging ophthalmoscopy in age-related macular degeneration. *Acta Ophthalmol*. 2023;101:e154–e166.